Characterizing Astrophysical Binary Neutron Stars with Gravitational Waves

Xing-Jiang Zhu (朱兴江)[1,2] and Gregory Ashton (艾格瑞)[1,2]

[1] School of Physics and Astronomy, Monash University, Clayton, VIC 3800, Australia; zhuxingjiang@gmail.com
[2] OzGrav: Australian Research Council Centre of Excellence for Gravitational Wave Discovery, Clayton, VIC 3800, Australia

Abstract

Merging binary neutron stars are thought to be formed predominantly via isolated binary evolution. In this standard formation scenario, the first-born neutron star goes through a recycling process and might be rapidly spinning during the final inspiral, whereas the second-born star is expected to have effectively zero spin at merger. Based on this feature, we propose a new framework for the astrophysical characterization of binary neutron stars observed from their gravitational wave emission. We further propose a prior for the dimensionless spins of recycled neutron stars, given by a gamma distribution with a shape parameter of 2 and a scale parameter of 0.012, extrapolated from radio pulsar observations of Galactic binary neutron stars. Interpreting GW170817 and GW190425 in the context of the standard formation scenario and adopting the gamma-distribution prior, we find positive support (with a Bayes factor of 6, over the nonspinning hypothesis) for a spinning recycled neutron star in GW190425, whereas the spin of the recycled neutron star in GW170817 is small and consistent with our prior. We measure the masses of the recycled (slow) neutron stars in GW170817 and GW190425 to be $1.34^{+0.12}_{-0.09}$ ($1.38^{+0.11}_{-0.11}$)$M_\odot$ and $1.64^{+0.13}_{-0.11}$ ($1.66^{+0.12}_{-0.12}$)$M_\odot$, with 68% credibility, respectively. We discuss implications for the astrophysical origins of these two events and outline future prospects of studying binary neutron stars using our framework.

Unified Astronomy Thesaurus concepts: Gravitational waves (678); Neutron stars (1108); Binary pulsars (153)

1. Introduction

The ground-based gravitational-wave interferometers Advanced LIGO (Aasi et al. 2015) and Advanced Virgo (Acernese et al. 2015) have discovered dozens of compact binary coalescence events (Abbott et al. 2019a, 2020a, 2020b, 2020c) and numerous candidates.[3] These include binary black holes, binary neutron stars (BNSs), and possibly neutron star–black hole mergers,[4] which are revolutionizing our understanding of the universe.

Current gravitational-wave inference methods (Veitch et al. 2015; Ashton et al. 2019; Biwer et al. 2019) label the two merging compact objects as primary and secondary, with corresponding masses $m_1 \geqslant m_2$. However, components of BNS mergers are expected to be of comparable masses, which makes the (m_1, m_2) parameterization inadequate. It has long been thought that neutron star (NS) masses in BNS systems are restricted within a narrow range around $1.35\,M_\odot$ (Özel et al. 2012; Kiziltan et al. 2013). Such a perception was gradually changed with a steadily increased sample of observed pulsars in Galactic BNSs in recent years. There are now 19 known Galactic BNS systems; 12 of them have masses measured for both stars (see Table 1 in Appendix A for details). The most asymmetric merging Galactic BNS has a mass ratio $q = 0.78$ (Ferdman et al. 2020), although see Andrews (2020) for a recent claim that 98% of merging BNSs are expected to have $q > 0.9$ if the Galactic BNS population is representative. Looking at all available precise NS mass measurements, which mostly come from observations of binary pulsars (e.g., Antoniadis et al. 2016; Alsing et al. 2018), the minimum and maximum are $1.17\,M_\odot$ (Martinez et al. 2015) and $2.14\,M_\odot$ (Cromartie et al. 2020), respectively. Whereas not necessarily corresponding to the natural extremes of NS masses, they provide a reasonable lower limit at $q \approx 0.55$ for BNS mergers.

The ability to measure the mass ratio of compact binary mergers through gravitational waves depends sensitively on our prior knowledge of the spins of the merging objects. For the first BNS merger event GW170817, Abbott et al. (2019b) found a 90% credible lower bound of $q = 0.53$ if both stars are allowed to possess extreme spins. Such a lower bound is comparable to the $q \approx 0.55$ limit arising from current pulsar mass measurements. Below, we describe a new astrophysically motivated framework, where the two stars in BNS mergers are distinguished by type[5] rather than by mass. This allows us to analyze NS mergers with an astrophysical prior.

It is believed that the BNS merger rate is dominated by the standard formation channel of isolated binary evolution (De Loore et al. 1975; Flannery & van den Heuvel 1975; Massevitch et al. 1976; Smarr & Blandford 1976; Kalogera et al. 2007; Postnov & Yungelson 2014; Tauris et al. 2017), since the merger rate of alternative dynamical formation is orders of magnitude lower (Phinney 1991; Bae et al. 2014; Belczynski et al. 2018; Ye et al. 2020). In the standard formation scenario, the two stars of the BNS system have distinct properties. The first-born NS is expected to undergo a recycling process where it gets spun up by accreting matter from its companion star (Alpar et al. 1982; Radhakrishnan & Srinivasan 1982; Srinivasan & van den Heuvel 1982; van den Heuvel 2017), prominently during the case-BB Roche–lobe overflow (Delgado & Thomas 1981; Tauris et al. 2015). The end product is a recycled NS, with a spin period of order 10 to 100 ms and low spin-down rate. The second-born NS, on the other hand, is "normal": it spins down quickly, in $\sim 10\,$Myr from a birth spin period of tens of milliseconds to $\mathcal{O}(1)$ s. For gravitational-wave analysis, the second-born NS is effectively nonspinning during the final inspiral, and hence termed the slow NS. In the astrophysical parameterization, the masses

---

[3] https://gracedb.ligo.org/superevents/public/O3/
[4] The recently published event, GW190814, contains either the lightest black hole or heaviest neutron star (Abbott et al. 2020c).

[5] We provide a brief overview of pulsar phenomenology and define our terminology in Appendix A.

(dimensionless spin) of the recycled and slow NSs are denoted as m_r (χ_r) and m_s (χ_s), respectively. We do not impose any ordering on m_r and m_s.

Among the Galactic BNS population, the Double Pulsar (J0737−3039A/B) is an excellent example for our *recycled* and *slow* labeling scheme for BNS mergers. It is unique, with both NSs being observed as radio pulsars (Burgay et al. 2003; Lyne et al. 2004): one is recycled with a spin period (P) of 22.7 ms and a spin-down rate ($\dot{P}$) of 1.76×10^{-18} s s^{-1}, and the other is slow with a spin period of 2.8 s and a spin-down rate of 8.92×10^{-16}. They are expected to merge in 86 Myr. There are another nine BNSs that will merge within a Hubble time. All pulsars but one observed in these BNSs are recycled, with spin periods from 17 to 76.5 ms, and spin-down rates from 1.6×10^{-19} to 8.6×10^{-18}. The exception is PSR J1906 +0746, which is a young pulsar with a spin period of 144 ms. It is spinning down quickly ($\dot{P} = 2 \times 10^{-14}$) and will become a slow pulsar when merging with its companion in 300 Myr (van Leeuwen et al. 2015).

The majority of known Galactic BNSs are found in the Galactic disk and can be described in the standard formation scenario (e.g., Tauris et al. 2017). Among 10 merging BNSs in the Galaxy, PSR B2127+11C is the only exception, being found in the globular cluster M15 (Anderson et al. 1990). Phinney & Sigurdsson (1991) and Prince et al. (1991) suggested that the original stellar companion of PSR B2127+11C might be replaced by another NS through a dynamical encounter, which also resulted in the ejection of the BNS to the outskirts of M15. It was estimated that the BNS merger rate from globular clusters similar to M15 can account for a significant fraction ($\sim$10%– 30%) of observed short gamma-ray bursts (Grindlay et al. 2006; Lee et al. 2010). However, Ye et al. (2020) found that dynamical interactions in globular clusters are dominated by black holes and thus make a negligible contribution to the overall BNS merger rate (see also Belczynski et al. 2018). Therefore, it is generally believed that the BNS merger rate inferred from observations by the LIGO/Virgo Collaboration (LVC; Abbott et al. 2017, 2020a) is dominated by the standard formation channel (Mapelli & Giacobbo 2018; Neijssel et al. 2019), although see Andrews & Mandel (2019) for speculation of a dynamical origin for several Galactic-disk BNSs with similar orbital characteristics to PSR B2127+11C.

Farrow et al. (2019) analyzed mass measurements of Galactic BNSs in the (m_r, m_s) framework and found modest evidence for distinct distributions of m_r and m_s, and a bimodal distribution of m_r. These features might be due to different supernova explosion mechanisms (Schwab et al. 2010; Pejcha et al. 2012) or the recycling process (but probably to a much lesser extent, see, e.g., Tauris et al. 2017). Farrow et al. (2019) demonstrated that dozens of new BNS observations, which are achievable with future observing runs of Advanced LIGO/Virgo and ongoing/new radio pulsar surveys in $\lesssim$5 yr, are required to draw firm conclusions. In this work, we extrapolate from observational properties of Galactic BNS systems to derive an astrophysical prior on χ_r. This will allow us to probe distributions of m_r and m_s through gravitational-wave observations.

The remainder of this paper is organized as follows. In Section 2, we derive an astrophysical prior distribution on χ_r, demonstrate the robustness of the $\chi_s = 0$ assumption, and briefly summarize our prior knowledge on spin tilt angles of recycled NSs in BNS systems. In Section 3, we apply the new population prior to the analysis of two BNS mergers published

so far—GW170817 (Abbott et al. 2017) and GW190425 (Abbott et al. 2020a)—using public data releases from LVC. We also propose a couple of novel tests for the dynamical formation hypothesis. Last, we discuss astrophysical implications from our analysis for both events and outline future prospects in Section 4.

2. Spins of Binary Neutron Stars

2.1. An Astrophysical Prior on the Dimensionless Spins of the First-born Recycled Neutron Stars

Here, we establish an astrophysical prior on the dimensionless spin magnitudes, χ_r, of recycled NSs in BNS systems, as measured in the final binary inspiral. Following Zhu et al. (2018), we extrapolate from the observed properties of 10 Galactic BNSs to a representative population of BNSs, each characterized by m_r, m_s, initial orbital period P_b and eccentricity, and P and $\dot{P}$ of the recycled NS at the birth of second NS. Observationally, the spin periods of recycled pulsars in Galactic-disk BNS systems appear to be correlated with their orbital periods (see Figure 1). To generate our birth BNS population, we make use of the following empirical P–P_b correlation (Tauris et al. 2015, 2017):

$$P = (36 \pm 14)(P_b/\text{days})^{0.4} \text{ ms}. \qquad (1)$$

The above equation was originally obtained by Tauris et al. (2017) in an empirical fit to 11 Galactic-field BNS systems, with a particular weight placed on the widest binary, PSR J1930−1852, which has a spin period of 186 ms and an orbital period of 45 days (Swiggum et al. 2015). In Figure 1, one can see that this correlation is supported by the up-to-date sample of observations. Since we are primarily interested in a reasonable prior on χ_r, we ignore the uncertainty on the correlation slope and hold it fixed at 0.4.

Equation (1) suggests that binaries born with tighter orbits tend to contain faster-spinning recycled NSs, which can be (qualitatively) attributed to a longer recycling process (see Tauris et al. 2017 for details). To obtain the distribution of P at merger, we follow the spin-down evolution of each recycled NS in our population from the birth of the BNS to binary merger. We adopt the standard magnetic dipole braking model (Goldreich & Julian 1969; Ostriker & Gunn 1969; Spitkovsky 2006) for spin-down evolution, and the formalism of Peters (1964) for gravitational-wave-driven binary orbital evolution. The initial spin-down rate is determined by assigning a log-normal distribution of magnetic field strength that covers the range of measurements for Galactic BNSs, given an NS equation of state or radius parameter. The magnetic field strength is assumed to be constant from binary birth to merger. Whereas magnetic field decay might occur for young NSs (Goldreich & Reiseneg- ger 1992) or for NSs undergoing the recycling process (Taam & van den Heuvel 1986; Romani 1990), it is thought to be unlikely for recycled NSs such as millisecond pulsars (Bransgrove et al. 2018). More details on the methodology and prescriptions of the BNS population can be found in Zhu et al. (2018).

The definition of $\chi \propto I/(m^2 P)$ means that there are three ingredients in the distribution of χ: (1) the distribution of spin periods (P), (2) the distribution of masses (m), and (3) the equation of state, which, together with m, determines the moment of inertia (I). To compute the moment of inertia, we make use of the empirical relation between $I/(mR^2)$ and m/R
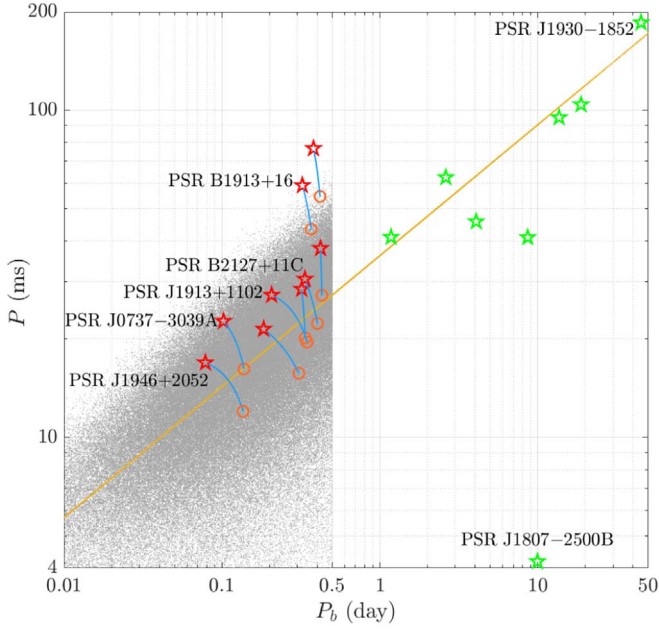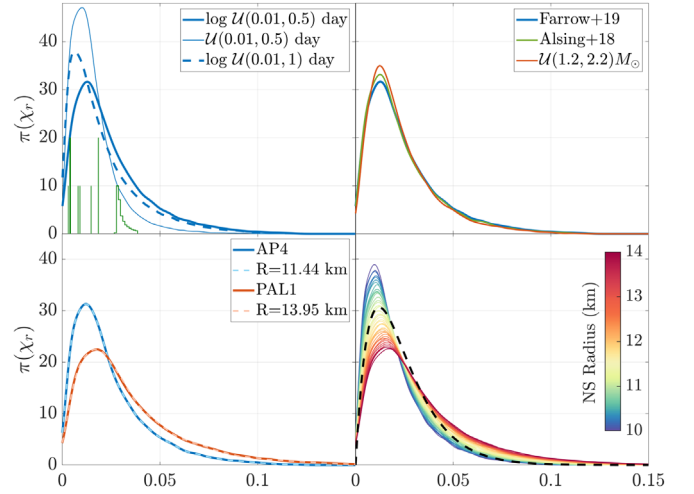
Figure 1. The P–P_b correlation (Equation (1)) for BNS systems formed via isolated binary evolution. Also shown are 17 Galactic BNSs that contain an observed recycled pulsar. Red (green) stars indicate merging (non-merging) systems. Orange circles mark plausible initial states (at the birth of the second NS) for merging systems, with blue lines showing the evolutionary tracks backward in time up to half the characteristic ages ($P/2\dot{P}$) of the recycled pulsars. Next to star symbols are listed names of some pulsars mentioned in the text. Grey dots in the background represent synthetic BNS systems in this work. Two BNSs in globular clusters are shown for completeness.

Figure 2. The probability distribution of the dimensionless spins $\pi(\chi_r)$ of recycled NSs in BNS systems. Top left: different initial binary orbital period distributions ($\mathcal{U}$—uniform distribution, and $\log \mathcal{U}$—uniform distribution on a $\log_{10}$ scale), along with expected χ during merger for nine recycled pulsars in merging Galactic BNSs (green lines, scaled to a coordinate height of 10 for each NS—a height of 20 indicates two pulsars having identical χ at merger). Top right: different mass distributions—Farrow+19 (Farrow et al. 2019), Alsing+18 (Alsing et al. 2018), and uniform between 1.2 and 2.2 $M_\odot$. Bottom left: two NS equations of state (AP4 and PAL1) and under the assumption that all NSs have the same radius ($R = 11.44$ km and 13.95 km). Note that there exist subtle differences between using an equation-of-state model and a single NS radius parameter; solid and dashed lines precisely overlap as a result of curve smoothing. Bottom right: distribution of χ_r for a range of NS radii from 10 to 14 km (colored lines), and the gamma distribution with a shape parameter of 2 and a scale parameter of 0.012 (black dashed line). We note that our spin distribution model shown here is qualitatively similar to more sophisticated population synthesis models (e.g., Chattopadhyay et al. 2020).

(with R being NS radius) found in Lattimer & Schutz (2005) for a range of realistic NS equations of state (see their Equation (12)). As a side note, we find that a more natural choice of prior would be on P, so that the mass distribution and NS equation of state can be simultaneously inferred with a population of events (e.g., Wysocki et al. 2020). Nevertheless, in what follows we describe a model for the distribution of χ_r that takes into account uncertainties in the distributions on P and m and the equation of state. This will provide insights into how much information about the NS mass distribution and equation of state can be extracted from spin measurements *alone* through hierarchical inference.

In Figure 2, we show the effect of different initial orbital period (P_b) distributions (top left panel), mass distributions (top right panel), and the NS equation of state (bottom two panels) on the distribution of χ_r. In our fiducial model, we assume a log-uniform distribution of P_b between 0.01 and 0.5 days. In comparison, the orbital periods of 10 merging Galactic BNSs range from 0.078 to 0.421 days. By applying the P–P_b correlation down to an orbital period of 0.01 days, the shortest initial spin period is about 4 ms. Overall, around 10% of recycled NSs have $P < 10$ ms at the birth of the second NS in our population. This makes our model conservative since theoretical modeling of standard BNS formation suggests that the first-born NS is usually only moderately recycled; Tauris et al. (2015) found a shortest spin period of 11 ms assuming an accretion efficiency of three times the Eddington limit during the case-BB Roche–lobe overflow.

Based on measurements of Galactic BNSs, we adopt a two-Gaussian distribution of m_r, peaking at 1.34 and 1.47 $M_\odot$, with widths of 0.02 and 0.15 $M_\odot$ and weights of 0.68 and 0.32,

respectively (Farrow et al. 2019); the distribution of m_s is uniform between 1.1 and 1.5 $M_\odot$. The distribution of m_s is only needed for calculation of the merger time and we find it has no impact on our results. Our fiducial choice of equation of state is AP4 (Lattimer & Prakash 2001).

In the top left panel of Figure 2, we also show the result for two alternative distributions of P_b: (a) uniform between 0.01 and 0.5 days (thin solid line) and (b) log-uniform between 0.01 and 1 days (thick dashed line). In comparison to our fiducial model (thick solid line), both (a) and (b) result in a smaller fraction of fast-spinning NSs, because recycled NSs have smaller initial spins in long-P_b binaries and the spin-down time is longer (meaning smaller residual spins at merger). Even though (a) and (b) may appear to provide a better fit to Galactic BNSs (shown as green lines), we choose our fiducial model because it allows a relatively larger fraction of fast spins. This is a conservative choice from the perspective of building a population prior. It is reasonable to believe a priori that the actual fraction of fast-spinning recycled NSs is greater than that of the *observed* Galactic BNS population because of at least three selection effects. The first two arise from the short orbital periods associated with fast recycled NS spins (i.e., the P–P_b correlation). Pulsars in these tight binaries are more difficult to detect in radio pulsar surveys because of severe Doppler smearing of pulse signals and their short merger times. A third one is the selection effect against short spin periods due to dispersion smearing of pulse signals by the interstellar medium, favoring the intermediate range from tens to hundreds of milliseconds (see, e.g., Figure 11 in Lazarus et al. 2015).

In the top right panel of Figure 2, we show the spin distribution for three mass models. In addition to the model of Farrow et al. (2019), we also consider: (1) the two-Gaussian model of Alsing et al. (2018) fitted to mass measurements of NSs in all binaries, peaking at 1.34 and 1.80 $M_\odot$, with widths of 0.07 and 0.21 $M_\odot$ and weights of 0.65 and 0.35, respectively; and (2) a uniform distribution between 1.2 and 2.2 $M_\odot$. It is apparent that the distribution of spin magnitude is insensitive to the mass model. In the bottom left panel, we show the distribution of χ_r for two equations of state—AP4 and PAL1, as investigated in Zhu et al. (2018), and assuming that all NSs have the same radius (11.44 km and 13.95 km, respectively). It can be seen that the effect of equation of state is completely captured by the radius parameter.

In the bottom right panel of Figure 2, we show the spin distribution (depicted in different colors) for a range of NS radii from 10 to 14 km—a plausible range allowed by current gravitational-wave and pulsar observations (Landry et al. 2020). As an arbitrary fit to the group of colored curves, the black dashed curve is given by the gamma distribution with a shape parameter of 2 and a scale parameter of 0.012. We propose this gamma distribution to be used as an astrophysical prior on χ_r in gravitational-wave data analysis. Once dozens or more BNS events are detected, we may be able to update the prior to reveal information encoded in the spin distribution as shown in Figure 2 (see also Zhu et al. 2018).

2.2. Can the Second-born Neutron Star Be Spinning at a Measurable Rate during the Final Binary Inspiral?

The spin period of pulsar B in the Double Pulsar system is 3 s, corresponding to $\chi_s \approx 10^{-4}$. PSR J1906+0746 is the only other young pulsar in merging Galactic BNS systems. Its spin period of 144 ms translates to $\chi_s \approx 0.003$. However, it is spinning down quickly, at 2×10^{-14}. By the time of binary merger (in 300 Myr), its dimensionless spin is expected to be well below 10^{-3}, which is effectively zero for gravitational-wave observations.[6] To examine the conditions under which the second-born NS can be spinning fast at merger, we conduct the following investigation.

The second-born NS in a BNS system inevitably spins down after its birth, due to the loss of rotational energy by powering magnetically driven plasma winds (Goldreich & Julian 1969; Contopoulos et al. 1999; Spitkovsky 2006). Its final spin period depends on the birth spin period P_0 and spin-down rate, and the spin-down time, which equals the binary merger time. As we show in the previous subsection, the dimensionless spin χ is largely determined by the spin period, since the spread in NS masses and radii can change χ by no more than $\approx 50\%$. We follow the spin-down evolution from birth to binary merger of a hypothetical NS. We assume a radius of $R = 12$ km, and set mass $m = 1.29\,M_\odot$ and initial spin-down rate $\dot{P} = 2 \times 10^{-14}$ to those of PSR J1906+0746. We consider two cases where the NS magnetic field strength either remains constant in this evolution or decays exponentially with a typical timescale τ_{decay} (see Appendix A in Zhu et al. 2018 for details).

Figure 3 shows lines of constant χ_s for a range of initial spin periods, merger times, and magnetic field decay timescales. In the upper panel, where the magnetic field is assumed not to be
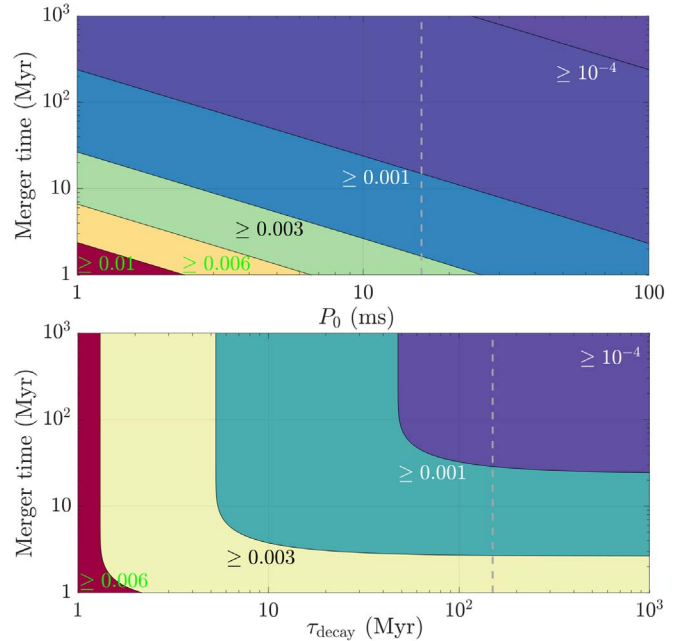
Figure 3. Lines of constant dimensionless spin (χ_s) for the second-born NS in the standard BNS formation scenario: P_0—the birth spin period, τ_{decay}—the magnetic field decay timescale. The initial spin-down rate is fixed at 2×10^{-14} in both panels. In the upper panel, the magnetic field strength is assumed to remain constant from the NS birth to binary merger, and the vertical line marks the shortest spin period, 16 ms, of known young pulsars (Marshall et al. 2004). In the lower panel, P_0 is fixed at 10 ms, and the vertical line indicates the typical decay timescale of 150 Myr found in Bransgrove et al. (2018).

decaying, one can see that two conditions need to be met for $\chi_s \gtrsim 0.003$—P_0 in the range of a few milliseconds and merger times shorter than 10 Myr. The vertical dashed line in this panel marks the spin period (16 ms) of PSR J0537−6910 (Marshall et al. 2004), the fastest-spinning young pulsar in the ATNF Pulsar Catalogue[7] (Manchester et al. 2005). In the lower panel, where P_0 is fixed at 10 ms, it becomes evident that $\tau_{decay} \lesssim 10$ Myr is required for $\chi_s \gtrsim 0.003$. However, that is unlikely given current understanding of NS magnetic field evolution. For example, the vertical line in the lower panel marks the typical decay timescale of 150 Myr found in Bransgrove et al. (2018) for young and hot NSs.

In summary, Figure 3 shows that the parameter space required for the second-born NS to be spinning at measurable rates during the final BNS inspiral is rather limited. There are three additional lines of argument for $\chi_s = 0$. First, the spin-down rate (of PSR J1906+0746) assumed in Figure 3 is low for $P_0 < 100$ ms. Pulsars with a shorter spin period than PSR J1906+0746's 144 ms generally have higher spin-down rates (e.g., $\dot{P} = 5 \times 10^{-14}$ for PSR J0537−6910). Second, by associating young pulsars with supernova remnants and thus obtaining independent age estimates, Popov & Turolla (2012) found that NS birth spin periods are likely to be between 10 and hundreds of milliseconds. Third, even though NSs might be born with spin periods of a few milliseconds, they are expected to spin down quickly (in $\lesssim 10$ yr) to $\gtrsim 10$ ms (Lorimer et al. 1993; Lai et al. 2001; Vink 2008). Therefore, we conclude that the second-born NS is effectively nonspinning for

---

[6] In comparison, the 90% credible upper bound on component spins of GW170817 under the low-spin ($\chi < 0.05$) prior is 0.04 (Abbott et al. 2019b). We discuss the measurement of NS spins with gravitational waves in detail in Appendix B.

[7] Refer to the Catalogue version 1.63, among 50 pulsars with $P_0 < 100$ ms and $\dot{P} > 10^{-16}$.

gravitational-wave observations, unless the merger time is $\ll 1$ Myr, which we do not consider in this study.

2.3. The Spin Tilt Angles of Recycled Neutron Stars

While six parameters are required to describe the spin vectors of two NSs in a binary merger, spin effects are primarily measurable in gravitational waves through two parameters (e.g., Abbott et al. 2019b and references therein): (1) the effective spin parameter $\chi_{\rm eff}$, which is the mass-weighted combination of spins along the orbital angular momentum vector $\boldsymbol{L}$; (2) the effective spin-precession parameter χ_p, which quantifies the spin components perpendicular to $\boldsymbol{L}$. By setting $\chi_s = 0$ and letting θ be the spin tilt angle of the recycled NS with respect to $\boldsymbol{L}$, it becomes evident that $\chi_{\rm eff} = m_r \chi_r \cos\theta/(m_r + m_s)$, and $\chi_p = \chi_r \sin\theta$ (if $m_r \geqslant m_s$) or $\chi_p = \chi_r \sin\theta (m_r/m_s)(3m_s + 4m_r)/(4m_s + 3m_r)$ (if $m_r < m_s$). Apart from χ_r, the key parameter is the spin tilt angle θ, for which we briefly summarize our prior knowledge below.

From a binary evolution perspective, the spin axis of a recycled NS gets aligned with orbital angular momentum during the recycling process (Hills 1983; Bhattacharya & van den Heuvel 1991), therefore the spin tilt angle is generally related to the supernova kick imparted to the second-born NS directed out of the orbital plane (Tauris et al. 2017). Bailes (1988) considered a range of BNS progenitors for PSR B1913 +16 and a Rayleigh distribution with a scale parameter of $150\,{\rm km\,s^{-1}}$ for the kick velocity, and showed that $\theta \lesssim 60°$ with $\gtrsim 90\%$ confidence. The spin tilt angle of the pulsar can be constrained by measuring the pulse profile variations induced by spin precession. For PSR B1913+16, θ was measured to be $18° \pm 6°$ by Kramer (1998). In the last decade, θ was constrained for three additional recycled pulsars in Galactic BNSs: $\theta < 3.2°$ for PSR J0737−3039A (Ferdman et al. 2013), $\theta = 27° \pm 3°$ for PSR B1534+12 (Fonseca et al. 2014), $\theta < 34°$ for PSR J1756−2251 (Ferdman et al. 2014).

Therefore, it is reasonable to believe that large spin tilt angles are unlikely a priori for recycled NSs in standard BNS systems. In the following section, we consider both aligned spins and isotropic spin orientation when we reanalyze GW170817 and GW190425 in our astrophysical framework. With the relaxed isotropic spin prior, we are able to compare the posteriors on θ against prior knowledge mentioned here. Unless otherwise specified, results presented hereafter assume isotropic spin orientation for the recycled NS.

3. Reanalysis of GW170817 and GW190425

Adopting our astrophysical parameterization of the masses and spins (m_r, m_s, χ_r, χ_s) and the spin priors derived in Section 2, we reanalyze the two BNS merger events detected by LIGO/Virgo: GW170817 and GW190425. We use the `IMRPhenomPv2_NRTidal` waveform model, which includes an effective description of spin-precession and tidal effects (Hannam et al. 2014; Khan et al. 2016; Dietrich et al. 2017a, 2019). In our prior, the detector-frame binary chirp mass is uniform in [1.18, 1.21] ([1.48, 1.495]) $M_\odot$ for GW170817 (GW190425) and the mass ratio m_s/m_r is uniform in [0.125, 8], with detector-frame component masses restricted in [1.0, 4.3] $M_\odot$. Note that the definition of mass ratio in our prior is necessary since we impose no ordering between m_r and m_s. Elsewhere in the paper, e.g., when comparing with the LVC results, we adopt the $q \leqslant 1$ convention. We find that our
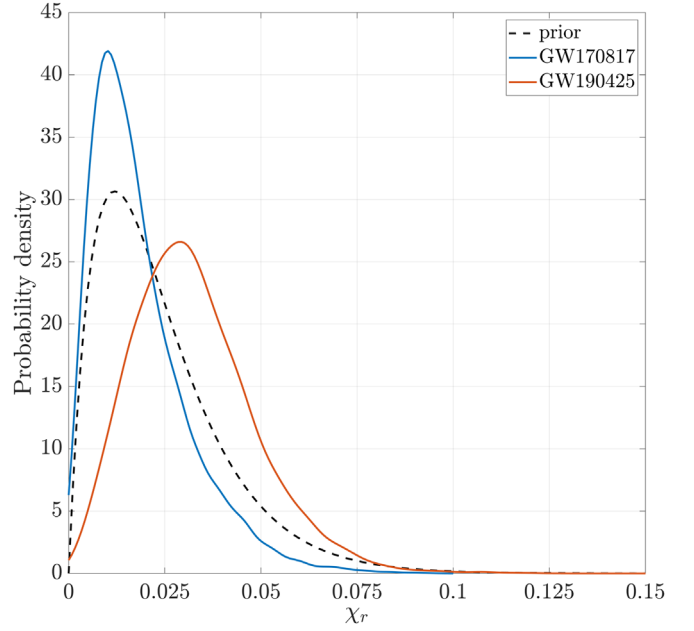

Figure 4. Posterior distributions of the dimensionless spins (χ_r) of recycled NSs in GW170817 and GW190425, derived under the astrophysical prior (black dashed line) and assuming aligned spins.

posteriors have no support near our prior limits. Priors for other source parameters are identical to those used in the LVC discovery papers (Abbott et al. 2017, 2020a); for GW170817, we fix the sky location to its host galaxy NGC 4993 (Abbott et al. 2017b).

Assuming aligned spins, we obtain a Bayes factor of 6 (0.8) between the spinning and nonspinning hypotheses for GW190425 (GW170817). This implies positive support for NS spins in GW190425, and that there is no evidence for or against spins in GW170817. Figure 4 shows the posterior distributions of χ_r, along with the prior. In accordance with Bayes factor results, the posterior of GW190425 moderately shifts toward larger spins, peaking at $\chi_r = 0.03$ in comparison to 0.012 for the prior; for GW170817 the posterior is similar to the prior, only shifting slightly toward lower spins.

Assuming a uniform prior for $\cos\theta$ between −1 and 1 (i.e., random spin orientation), Figure 5 shows the posterior probability densities of χ_r with respect to the orbital angular momentum $\boldsymbol{L}$ for GW170817 and GW190425, on the left and right half-disks, respectively. We find the spin in GW170817 is only weakly constrained, disfavouring anti-alignment with $\boldsymbol{L}$. The weak constraint on θ is unsurprising for GW170817 because of small spins. Given its high signal-to-noise ratio (32.4), this adds further weight to our finding that the recycled NS in GW170817 is only mildly spinning. On the other hand, the spin tilt angle can be constrained to be $\lesssim 60°$ for GW190425, with strongest support below 30°. This agrees well with astrophysical expectations presented in Section 2.3.

Figure 6 shows the joint posterior distributions of (m_r, m_s) for GW170817 and GW190425, along with 10 merging Galactic BNSs (Farrow et al. 2019). We find that both GW170817 and GW190425 are likely to be equal-mass binary mergers. The masses of the recycled (slow) NSs are measured to be $1.34^{+0.12}_{-0.09}$ ($1.38^{+0.11}_{-0.11}$) $M_\odot$ and $1.64^{+0.13}_{-0.11}$ ($1.66^{+0.12}_{-0.12}$) $M_\odot$, with
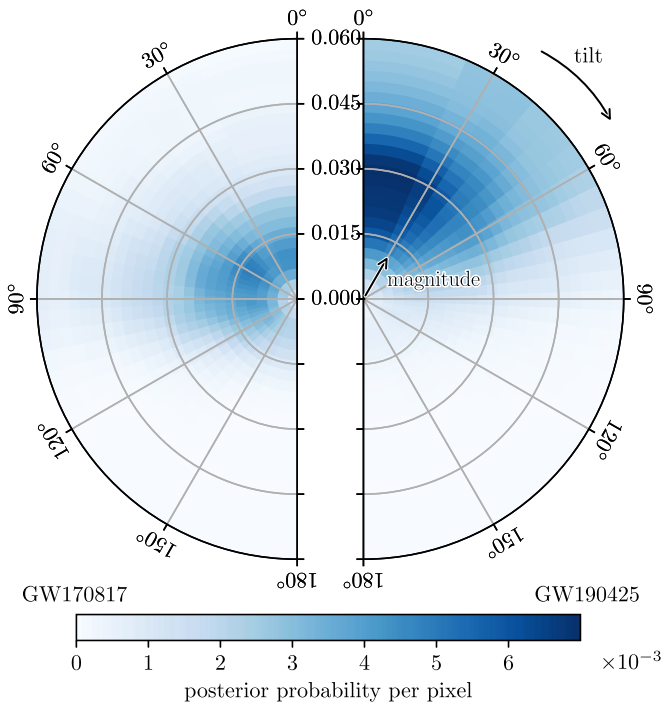
Figure 5. Posterior probability densities of χ_r in GW170817 (left) and GW190425 (right), with respect to the orbital angular momentum L. This is shown for the astrophysical spin prior using the `IMRPhenomPv2_NRTidal` waveform at a reference frequency of 20 Hz. A tilt angle of $0°$ indicates alignment with L.

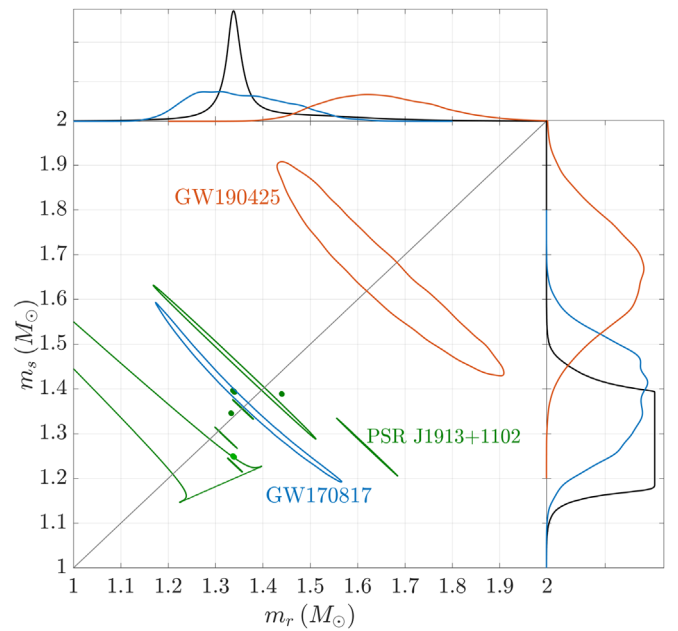**Figure 6.** Posterior distributions (shown as 90% credible regions) of NS masses (m_r and m_s) of GW170817 and GW190425, along with those for 10 merging Galactic BNSs (green lines). Due to high measurement precision, four Galactic BNSs are indicated as dots in the figure. One-dimensional marginalized distributions are given in the small panels on the top and right; black curves illustrate the posterior predictive distributions based on the Galactic BNS population (Farrow et al. 2019), where m_r and m_s follow a two-Gaussian distribution and a uniform one, respectively.

68% credibility, for GW170817 and GW190425, respectively. Reordering (m_r, m_s) into (m_1, m_2), we obtain slightly improved constraints on the mass ratio (defined as $q \leqslant 1$). For GW170817 (GW190425), our 90% credible lower bound on q is 0.79 (0.80), in comparison to 0.73 (0.78) by LVC[8] assuming the low-spin prior ($\chi < 0.05$). We provide a comprehensive comparison with LVC results in Appendix B.

In the one-dimensional marginal distribution plots of Figure 6, we show as black lines the posterior predictive distributions of m_r and m_s derived in Farrow et al. (2019) for Galactic BNS systems. We find the measurements of m_r and m_s for GW170817 are fully consistent with the Galactic BNS population. The measured m_r in GW190425 is broadly consistent (at the 18% confidence level) with the posterior predictive distribution. It falls under the secondary peak (at 1.47 $M_\odot$ with a width of 0.15 $M_\odot$) of the Galactic model, and is similar to $1.62 \pm 0.03\,M_\odot$ of PSR J1913+1102 (Ferdman et al. 2020)—the most massive recycled pulsar in Galactic BNS systems. However, the measurement of m_s of GW190425 is inconsistent with the Galactic population ($<1.5\,M_\odot$) at the 95% confidence level.

3.1. Test of the Dynamical Formation Hypothesis

Our priors on NS spins derived in Section 2 are valid only for the standard BNS formation channel. While current estimates of merger rate suggest that nearly all BNS mergers should be formed via the standard channel, one detected event outside the astrophysical prior proposed in this work would indicate a new origin. For example, in our prior, $\chi \gtrsim 0.05$ is relatively rare (8%), which arises from the theoretical

expectation that the first-born NS is usually only moderately recycled. However, a dynamically formed BNS could contain a fully recycled millisecond NS ($\chi \sim 0.1$–0.2). If both NSs were found to exhibit measurable spins, it would be "smoking-gun" evidence for a dynamically formed BNS containing two recycled NSs,[9] because that is extremely unlikely in standard BNS formation (see Section 2.2).

Since our analysis finds no support for measurable spins in GW170817, we only consider alternative possibilities for GW190425. For this purpose, we adopt a uniform prior between 0 and 0.1 for χ, where the upper end corresponds to a spin period of 3.6 (6.0) ms for an NS radius of 10 (14) km, for $m = 1.65\,M_\odot$. Note that PSR 1807−2500B, in the globular cluster NGC 6544, has a spin period of 4.19 ms (Lynch et al. 2012). It is the fastest-spinning recycled pulsar in Galactic BNS systems, but the binary ($P_b = 10$ days) is not expected to merge within the age of the universe.

We find a Bayes factor of 2 between the double-spinning and single-spinning hypotheses for GW190425 (under the same uniform prior for χ), and a Bayes factor of 1.3 between the uniform prior and astrophysical prior for the single-spinning hypothesis. These small Bayes factors imply that the data are insufficient to disentangle these possibilities. It is also worth mentioning that the Bayes factor needs to be weighted by prior odds, which are small for the dynamical formation hypothesis. Figure 7 shows the posterior probability densities for the single-spinning (left) and double-spinning (right) configurations. In the left panel, the left and right half-disks correspond to the uniform prior and astrophysical prior, respectively. Note

---

[8] We obtained the LVC lower bounds directly from the published posterior samples (The LIGO Scientific Collaboration & The Virgo Collaboration 2020). The lower bound for GW190425 was rounded to 0.8 in Abbott et al. (2020a).
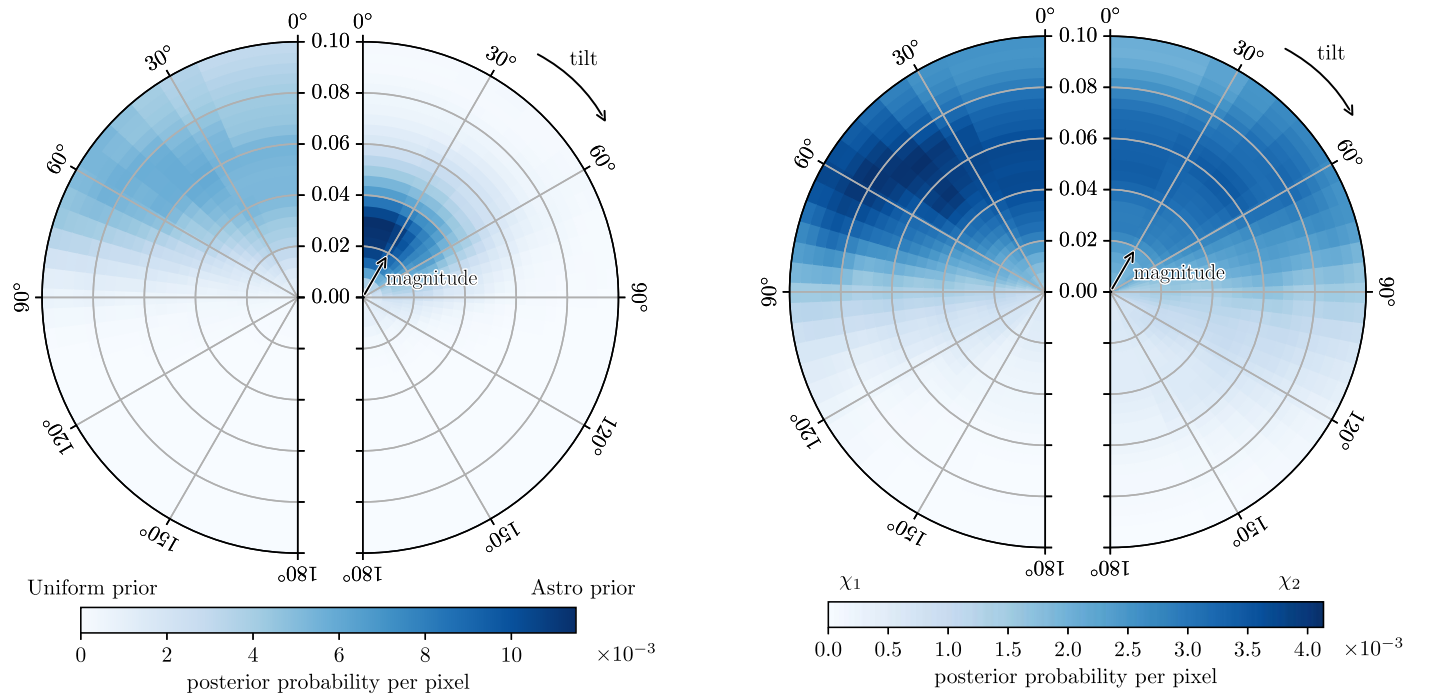
[9] If formed through three-body interactions, the captured NS could also be an isolated slow NS. Therefore, the single-spinning feature is not unique to the standard formation channel.

Figure 7. Posterior probability densities of NS spins with respect to the orbital angular momentum for GW190425. The left panel is for the recycled NS (χ_r), using two different priors, uniform between 0 and 0.1, and the astrophysical prior derived in Section 2.1; note that the posterior for the astrophysical prior was already shown in Figure 5, but with a different magnitude range. The right panel is for component spins χ_1 and χ_2, of the primary and secondary NSs, respectively.

that in all cases except the one using the astrophysical prior, each pixel in the plot has equal prior probability. From this test, we conclude that for GW190425: (1) anti-aligned spins (a tilt angle of ~180°) are strongly disfavoured; (2) assuming only one NS is spinning, its spin tilt angle is ≲60°.

4. Implications and Future Prospects

It is generally believed that the BNS merger rate is dominated by the standard formation channel of isolated binary evolution. We demonstrate that a generic feature for standard BNS formation is that the second-born NS is effectively nonspinning during the final merger. The first-born NS, on the other hand, can get spun up during a recycling process and is likely to retain significant spin at merger. This motivates us to propose a new *recycled* and *slow* labeling scheme, which also solves the dilemma of the primary–secondary parameterization in measuring BNS mergers.

We further propose a population prior on the dimensionless spins (χ_r) of recycled NSs by extrapolating pulsar spin measurements of 10 Galactic BNS systems to a wide range of initial orbital configurations. Such an extrapolation is made possible by the empirical correlation between the initial BNS orbital period (P_b) and the spin period (P) of the recycled NS, given by Equation (1) and illustrated in Figure 1. This relation directly results in a correlation between BNS merger times and the final spins of recycled NSs, as shown in Figure 8. It can be understood as follows. Shorter P_b implies a faster-spinning recycled NS, which also has a shorter spin-down time as determined by the merger time. There is potentially one extra factor (not included in our population modeling) that can strengthen such a correlation—a recycling spin-up process could reduce the NS spin-down rate. By approximating the equilibrium spin period of a magnetized NS in the accretion process with the Kepler orbital period at the Alfvén radius
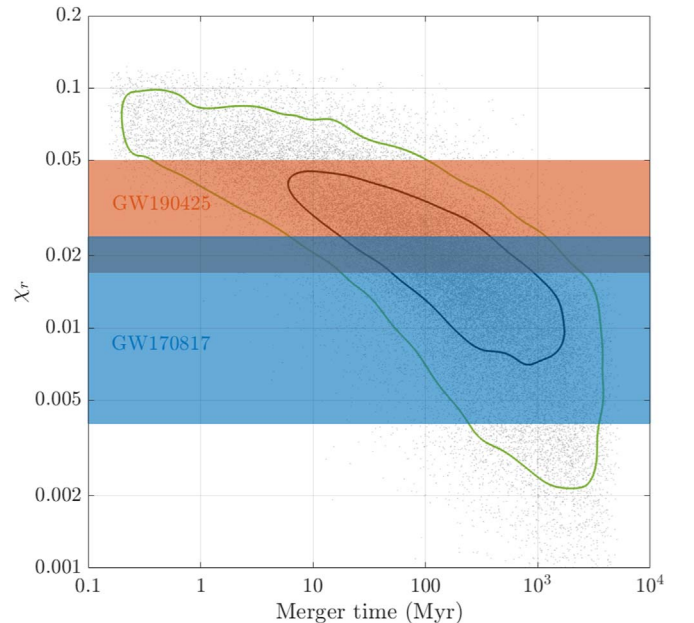
Figure 8. The correlation between BNS merger times and the dimensionless spins (χ_r) of recycled NSs measured during the final binary inspiral. The two horizontal bands mark the 68% credible intervals of the posteriors shown in Figure 4 for GW170817 and GW190425. Black and green curves enclose 50% and 90% of our population prior in the fiducial model described in Section 2.1, respectively.

(Ghosh & Lamb 1979), and assuming that the NS loses its rotational energy through dipolar electromagnetic radiation, there exists a spin-up relationship $\dot{P} \sim P^{4/3}$ (e.g., Arzoumanian et al. 1999). Observationally, fully recycled pulsars have lower spin-down rates than recycled pulsars in Galactic BNS systems. See Figure 9 in Appendix A for illustrations.

After accounting for uncertainties in NS mass distribution and equation of state, as well as selection effects in radio pulsar surveys, we find that a representative distribution of χ_r can be approximated by a gamma distribution with a shape parameter of 2 and a scale parameter of 0.012. Adopting the recycled–slow parameterization and the population prior on χ_r, we reanalyze public LVC data for GW170817 and GW190425. We find no support of measurable spins in GW170817, and modest evidence of spin for GW190425 with a Bayes factor of 6. We discuss the implications of our analysis for GW170817 (Section 4.1) and GW190425 (Section 4.2). Note in Figure 8 that significant uncertainties exist both for the correlation between spin and merger time and for our spin measurements. Therefore, we use the plot to make some qualitative (instead of quantitative) statements on the astrophysical origins of those two events. After that, we outline future prospects of studying BNS mergers using our framework.

4.1. Implications for GW170817

We show that the recycled NS in GW170817 is only mildly or even slowly spinning. The small spin implies a relatively long merger time as can be seen in Figure 8. Note that the sharp turnoff of merger time at $\sim 6\,\mathrm{Gyr}$ is due to a cut at $P_b = 0.5\,\mathrm{days}$ applied in our population modeling, which was chosen to derive a conservative prior on χ_r (see Section 2.1 for details). With such a caveat in mind, our result is consistent with the finding of Blanchard et al. (2017), who estimated a merger time between 6.8 and 13.6 Gyr (90% confidence) from the star formation history of its host galaxy NGC 4993.

We find that the two stars of GW170817 have comparable masses, around $1.35\,M_\odot$. The mass ratio is constrained to be above 0.79 with 90% credibility. Recently, Ferdman et al. (2020) proposed that around 2%–30% of BNS mergers are asymmetric, similar to the Galactic BNS system containing PSR J1913+1102 ($q = 0.78 \pm 0.03$), and that GW170817 might be one such merger with large mass asymmetry. Similar suggestions were made earlier, mostly to explain the ejecta associated with the kilonova accompanying GW170817 at optical and near-infrared wavelengths (e.g., Gao et al. 2017; Pankow 2018). Specifically, Pankow (2018) argued that the low mass ratio, $q \sim 0.65$, required to explain kilonova ejecta via a dynamical origin (Abbott et al. 2017a; Dietrich et al. 2017b), implies a tension between GW170817 and the Galactic BNS population. However, Metzger et al. (2018) showed that the dynamical hypothesis fails to simultaneously explain the quantity, velocity and composition of the ejecta responsible for the luminous optical (blue) kilonova emission. For alternative ejecta sources such as magnetar winds (Metzger et al. 2018) or accretion disk outflow (Siegel & Metzger 2018), no stringent constraint can be placed on the mass ratio of GW170817 from kilonova observations.

In short, we conclude that GW170817 is a canonical BNS merger with vanilla masses ($\approx 1.35\,M_\odot$) and contains a mildly spinning NS.

4.2. Implications for GW190425

The large total mass $3.3^{+0.1}_{-0.1}\,M_\odot$ of GW190425 is inconsistent with the *observed* Galactic BNS population. Abbott et al. (2020a) performed a simple Gaussian fit to measurements of 10 merging Galactic BNS systems and computed the inconsistency to be at the 5σ level. We found that when including

uncertainties of model parameters for the mass distributions of Galactic BNSs, e.g., comparing to the posterior predictive distribution shown in Figure 5 of Farrow et al. (2019), the inconsistency is somewhat alleviated, to the 3σ level.

Our analysis of GW190425 adds several pieces of information to that of Abbott et al. (2020a). First, modest evidence of a relatively fast-spinning recycled NS points to a merger time of $\lesssim 100\,\mathrm{Myr}$ (Figure 8). Second, the constraint on the spin tilt angle $\lesssim 60^\circ$ is consistent with the standard formation scenario. Third, our measurements of (m_r, m_s), both around $1.65\,M_\odot$, might provide additional clues to investigation of this event within the standard formation scenario. The remaining question is, why has no such *massive* BNS been observed before? Population synthesis models are capable of reproducing the high mass of GW190425 (e.g., Kruckow 2020; Mandel et al. 2020), but it is unclear how the above question should be tackled. We discuss two specific proposals below.

Romero-Shaw et al. (2020) proposed that a viable formation pathway for GW190425 is the unstable case-BB mass transfer process (Dewi & Pols 2003; Ivanova et al. 2003), which can create BNS systems in ultratight orbits ($P_b \lesssim 1\,\mathrm{hr}$). These fast-merging binaries are nearly invisible in radio pulsar surveys due to selection effects mentioned in Section 2.1. The large mass is a result of a survival effect, because an immediate BNS progenitor (an NS–helium star binary) in a wide orbit could have produced a massive BNS but it would get disrupted during the final supernova explosion (assuming the supernova kick is proportional to the resultant NS mass).

Safarzadeh et al. (2020) argued that the fast-merging channel is somewhat disfavoured, because it should contribute $\lesssim 10\%$ of the overall BNS merger rate, whereas the inferred merger rates based on GW170817 and GW190425 are comparable. They invoked a correlation between NS mass and magnetic field, namely that massive NSs are born with either too weak or too strong magnetic fields and thus are undetectable as pulsars. The authors acknowledged the observational evidence of massive pulsars in binaries with white-dwarf companions (e.g., Cromartie et al. 2020) and suggested that those systems may provide clues to understanding the origin of GW190425.

Given these unknowns, we have searched for evidence of dynamical formation for GW190425, namely, two fast-spinning NSs or only one spinning but with a large spin outside our prior. Unfortunately, the Bayes factors are not informative enough to tell these possibilities apart, mostly because of the relatively low signal-to-noise ratio (12.9). Nevertheless, such a test will prove useful in revealing the formation pathways of future BNS events.

It is worth mentioning that with $10 + 2$ observations, we are likely to be in the regime of small-number statistics. When comparing component masses of GW190425 to those of the Galactic population, we find the tension mostly lies in the mass of the slow NS, with a reduced level of inconsistency (2σ). Additionally, one has to keep in mind that high-mass BNS mergers are favored in gravitational waves because the detectable volume scales as $\mathcal{M}^{5/2}$ (with $\mathcal{M}$ being binary chirp mass), but they are selected against in radio because the binary lifetime scales as $\mathcal{M}^{-5/3}$.

In short, our analysis shows that GW190425 is consistent with being formed in a tight orbit (with a merger time $\lesssim 100\,\mathrm{Myr}$), including a fast-spinning recycled NS ($\chi \sim 0.03$, or $P \sim 15\,\mathrm{ms}$) with a spin tilt angle $\lesssim 30^\circ$. Future gravitational-

wave observations or radio pulsar surveys may soon unravel its "mass mystery".

4.3. Future Prospects

Gravitational-wave observations are the major driving force in refining our understanding of the formation of coalescing compact binaries. With planned upgrades of Advanced LIGO/ Virgo detectors and the operation of an enlarged global network, we are likely to see weekly detections of BNS mergers within the next five years (Abbott et al. 2018). This will usher in a new golden era in studying the formation and evolution of BNS systems. In parallel, the pace of discovery of relativistic binary pulsars has been readily accelerating in the last few years, doubling the sample size of known Galactic BNS systems. The radio BNS population is likely to grow significantly further, particularly thanks to new pulsar discovery and timing machines such as MeerKAT (Bailes et al. 2020) and FAST (Zhang et al. 2019; Cameron et al. 2020).

We propose a new framework for the analysis of gravitational-wave data from BNS mergers, based on the generic single-spinning feature found in the standard BNS formation scenario. This framework naturally links gravitational-wave observations to radio pulsar observations and theoretical population syntheses.

We also develop a population prior for the dimensionless spins χ_r of the spinning recycled NS, using the spin period–orbital period (P–P_b) correlation and with simple assumptions on binary orbital characteristics. There are several directions worthy of further investigations.

First, we demonstrate that there exists a correlation between BNS merger times and the dimensionless spins of recycled NSs at the final inspiral. Such a correlation can be further refined with a detailed modeling of the spin-up process and using more realistic distributions of initial binary orbital periods and eccentricities. Second, it would be interesting to examine where the P–P_b correlation ceases to be applicable. In our model, we extrapolate this correlation from the shortest observed P_b of 0.078 day to 0.01 day (for the sake of conservativeness), which results in a long tail beyond $\chi_r \approx 0.05$. A more informed upper end for χ_r would help to identify atypical NSs in BNS mergers. Third, we demonstrate that the distribution of χ_r is insensitive to NS mass distribution, but uniformly affected by the NS equation of state through the NS radius parameter. Such insights could guide future work that aims to constrain the NS spin/mass distributions and the equation of state simultaneously via hierarchical inference.

The astrophysical framework proposed in this work will enable future gravitational-wave observations to determine whether or not the first and second-born NSs follow different mass distributions. This will in turn have significant implications for supernova explosion mechanisms involved in BNS formation. Once dozens of BNS mergers are detected, such a prior will also enable the measurement of the typical spin tilt angle of the recycled NS, which encodes information about the magnitudes of supernova kicks applied to the second-born NS. A population of $\mathcal{O}(>100)$ detected events will update the prior and reveal information about the NS equation of state, the distribution of initial BNS orbital periods, and potentially magnetic field decay (if it exists).

Finally, we outline a couple of novel tests based on NS spins to probe the formation pathways of BNS mergers. We find that a detected BNS event with measurable spins in both stars would be "smoking-gun" evidence for dynamical formation. On the flip side, a dynamically formed BNS is also likely to contain a slow NS, which could originally be an isolated NS and later be captured via dynamical interactions. We find no support for or against either of the above two scenarios for GW190425 due to its relatively low signal-to-noise ratio. If indeed the dynamical formation channel is not as ineffective as currently thought in producing BNS mergers, which could be confirmed via radio pulsar observations in the meantime, the NS spin tests within our framework may prove instrumental in future gravitational-wave observations.

Appendix A
Pulsar Phenomenology and Galactic Binary Neutron Stars

Here we briefly summarize pulsar phenomenology relevant to BNS systems and explain some terminology used in this work through the classic P–$\dot{P}$ diagram (Figure 9). We refer interested readers to, e.g., the book by Lorimer & Kramer (2005) for an in-depth review.

Generally, NSs are believed to be born somewhere in the top left corner of the P–$\dot{P}$ diagram. Adopting the standard magnetic dipole braking model and assuming no magnetic field decay, an NS evolves along a line of constant magnetic field strength toward the bottom right (parallel to purple lines in Figure 9). For an NS born with a spin period of $\mathcal{O}(10)$ ms, it takes ~ 10 Myr to spin down to a period of $\mathcal{O}(1)$ s.

Pulsars inside the major cloud around $P \sim 1$ s and $\dot{P} \sim 10^{-15}$ in Figure 9 are usually referred to as *normal* or *young* pulsars. They are mostly isolated pulsars. The secondary cloud, with P between 1 and ~ 10 ms and $\dot{P} \sim 10^{-20}$, contains what are usually called millisecond pulsars. Pulsars in Galactic BNSs (shown as star symbols in Figure 9) are mostly located in between the two clouds, except for three young pulsars and one millisecond pulsar. Most pulsars with $P < 200$ ms and $\dot{P} < 10^{-16}$ are found to be in binary systems, which are collectively referred to as recycled pulsars. Depending on their spin periods, we adopt the following terminology in this paper: mildly recycled ($P \gtrsim 80$ ms), moderately recycled (10 ms $\lesssim P \lesssim 80$ ms), and fully recycled ($P \lesssim 10$ ms).

Table 1
Properties of 19 Known Galactic BNS Systems

Pulsar Name	P (ms)	χ	$\dot{P}(10^{-18})$	P_b (day)	e_0	T_m (Gyr)	m_r ($M_\odot$)	m_s ($M_\odot$)	Reference
J1946+2052	16.96	0.031	0.92	0.078	0.064	0.046	$m_{tot} = 2.50 M_\odot$		Stovall et al. (2018)
J1757−1854	21.50	0.023	2.63	0.184	0.606	0.076	1.338	1.395	Cameron et al. (2018)
J0737−3039A	22.70	0.022	1.76	0.102	0.088	0.086	1.338	⋯	Kramer et al. (2006)
J0737−3039B	2773	10^{-4}	892	0.102	0.088	0.086	⋯	1.249	Kramer et al. (2006)
J1913+1102	27.29	0.016	0.16	0.206	0.090	0.470	1.62	1.27	Ferdman et al. (2020)
J1756−2251	28.46	0.017	1.02	0.320	0.181	1.656	1.341	1.230	Ferdman et al. (2014)
B2127+11C	30.53	0.016	4.99	0.335	0.681	0.217	1.358	1.354	Jacoby et al. (2006)
B1534+12	37.90	0.013	2.42	0.421	0.274	2.734	1.333	1.346	Fonseca et al. (2014)
B1913+16	59.03	0.008	8.63	0.323	0.617	0.301	1.440	1.389	Weisberg et al. (2010)
J0509+3801	76.54	0.006	7.93	0.380	0.586	0.574	1.34	1.46	Lynch et al. (2018)
J1906+0746	144.1	0.003	20268	0.166	0.085	0.308	1.322	1.291	van Leeuwen et al. (2015)
J1807−2500B	4.19	0.117	0.08	9.957	0.747	10^3	1.366	1.206	Lynch et al. (2012)
J1518+4904	40.93	0.012	0.03	8.634	0.249	10^4	$m_{tot} = 2.72 M_\odot$		Janssen et al. (2008)
J1829+2456	41.01	0.013	0.05	1.176	0.139	55	1.295	1.310	Haniewicz et al. (2020)
J0453+1559	45.78	0.010	0.19	4.072	0.113	10^3	1.559	1.174	Martinez et al. (2015)
J1411+2551	62.45	0.008	0.10	2.616	0.170	466	$m_{tot} = 2.538 M_\odot$		Martinez et al. (2017)
J1753−2240	95.14	0.005	0.97	13.64	0.304	10^4	⋯	⋯	Keith et al. (2009)
J1811−1736	104.2	0.004	0.90	18.78	0.828	10^3	$m_{tot} = 2.57 M_\odot$		Corongiu et al. (2007)
J1930−1852	185.5	0.003	18.0	45.06	0.399	10^5	$m_{tot} = 2.59 M_\odot$		Swiggum et al. (2015)
J1755−2550	315.2	0.001	2430	9.696	0.089	10^3	⋯	⋯	Ng et al. (2018)

Note. The properties listed include the spin period (P), dimensionless spin (χ) and spin-down rate ($\dot{P}$) of the pulsar, binary orbital period (P_b), orbital eccentricity (e_0), and merger time T_m. Also listed are the masses of the recycled NS (m_r) and slow NS (m_s) in the binary, or the binary total mass (m_{tot}). The systems are ordered based on pulsar spin periods, with merging (non-merging) binaries listed in the top (bottom) half. For 12 entries with mass measurements for both stars, m_r is the mass of the recycled pulsar, except PSR J1906+0746, which is a young pulsar (labeled as m_s and its companion as m_r). For two globular-cluster pulsars (B2127+11C and J1807 −2500B), their undetected companions could be either young or recycled NSs. In their respective references, PSRs J1906+0746, J1807−2500B, J1753−2240, and J1755−2550 were suggested to be likely in BNS systems, but their undetected companion stars could also be white dwarfs.
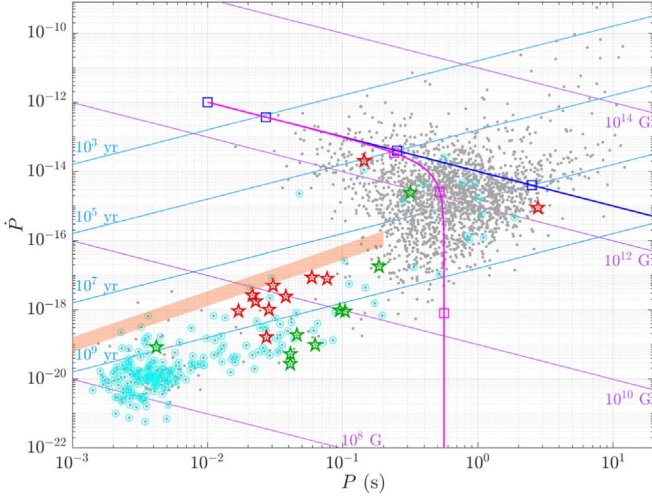

Figure 9. The pulsar P–$\dot{P}$ diagram based on the ATNF Pulsar Catalogue Version 1.63. Pulsars are plotted as gray dots, with cyan circles indicating binary systems. Red (green) stars mark pulsars in merging (non-merging) Galactic BNS systems. Also shown are lines of constant characteristic age $P/(2\dot{P})$ (light blue) and constant surface magnetic field strength $3.2 \times 10^{19}(P\dot{P})^{1/2}$ (G) (purple lines). As an illustration, the blue and pink lines mark the evolution of a hypothetical NS, with $P = 10$ ms and $\dot{P} = 10^{-12}$ at birth, assuming no magnetic field decay and an exponential field decay scenario with a typical timescale of 1 Myr, respectively. Blue squares indicate $\{0, 10^3, 10^5, 10^7\}$ yr after birth. Pink squares indicate $\{0.1, 1, 5\}$ Myr after birth. The orange shaded band represents the spin-up relation $\dot{P} = (1.1 \pm 0.5) \times 10^{-15}P^{4/3}$ (Ghosh & Lamb 1979; Arzoumanian et al. 1999), which approximately indicates the equilibrium spin periods of the spin-up accretion process. Note the general trend that faster-spinning recycled pulsars also have lower spin-down rates.

Appendix B
Comparison with LVC Results under the Low-spin Prior

In this section, we compare our results to the public data release of the LVC under the (m_1, m_2) parameterization. (GW170817 data are available at https://dcc.ligo.org/public/ 0150/P1800061/011/, and GW190425 at https://dcc.ligo. org/LIGO-P2000026/public.) Specifically, we compare to LVC results based on the low-spin prior, with component spin magnitudes $\chi_{1,2}$ uniformly distributed between 0 and 0.05. The limit in this prior corresponds to the dimensionless spin of the fastest-spinning pulsar J1946+2052 (Stovall et al. 2018) in *known* merging Galactic BNS systems, whereas the high-spin prior ($\chi_{1,2} < 0.89$) is an unconstrained prior with an upper end that is a technical limit imposed by available rapid waveform models (e.g., Abbott et al. 2017).

Our astrophysical spin prior within the (m_r, m_s) paradigm improves on the simple LVC low-spin prior in two ways. First, it incorporates the general expectation that the second-born NS is effectively nonspinning at merger for the standard BNS formation scenario. We denote this NS as the slow NS and set $\chi_s = 0$. Second, for the first-born recycled NS, we make use of the empirical P–P_b correlation, given in Equation (1), which is derived by fitting pulsar measurements of Galactic BNSs within the framework of theoretical modeling of standard BNS formation (Tauris et al. 2015, 2017). By further assuming a log-uniform distribution for the initial BNS orbital period P_b, our model accounts for the likely distribution of dimensionless spins (χ_r) of the recycled NSs for BNS mergers. Our prior extends beyond the LVC low-spin limit, with 8% probability
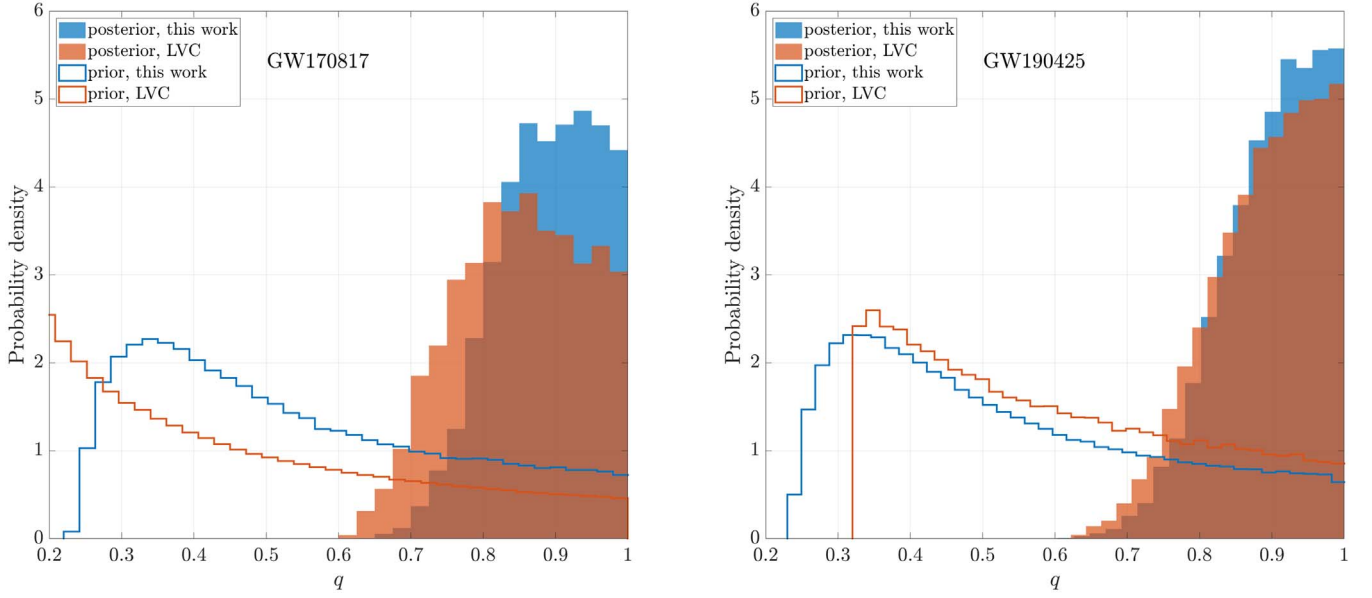
Figure 10. Posterior probability distributions of the mass ratio (q) for GW170817 (left) and GW190425 (right), along with the prior distributions. We compare results from this work to the public data release by the LVC. The LVC mass priors are as follows. For GW170817, the detector-frame component masses are uniform in [0.5, 7.7] $M_\odot$, with $\mathcal{M}^{\rm det}$ restricted in [1.184, 2.168] $M_\odot$ (Abbott et al. 2019b). For GW190425, the detector-frame component masses are uniform in [1.0, 5.31] $M_\odot$, with $\mathcal{M}^{\rm det}$ restricted in [1.485, 1.490] $M_\odot$ (Abbott et al. 2020a). Both the LVC mass priors and ours are chosen for technical reasons. While the two sets of priors are different, we note that our effective priors on q are nearly identical to those of the LVC for both events within the range spanned by the posterior distributions.

Table 2
Measured Source Parameters of GW170817 and GW190425 from This Work Compared to Those Published by the LVC

|		$\mathcal{M}^{\rm det}$	$\mathcal{M}$	$m_{\rm tot}$	q	$\chi_{\rm eff}$
GW170817	This work	$1.1975^{+0.0001}_{-0.0001}\,M_\odot$	$1.187^{+0.004}_{-0.002}\,M_\odot$	$2.73^{+0.02}_{-0.01}\,M_\odot$	(0.79, 1)	$0.00^{+0.01}_{-0.01}$
	LVC	$1.1975^{+0.0001}_{-0.0001}\,M_\odot$	$1.186^{+0.001}_{-0.001}\,M_\odot$	$2.73^{+0.04}_{-0.01}\,M_\odot$	(0.73, 1)	$0.00^{+0.02}_{-0.01}$
GW190425	This work	$1.4867^{+0.0003}_{-0.0003}\,M_\odot$	$1.44^{+0.02}_{-0.02}\,M_\odot$	$3.31^{+0.05}_{-0.05}\,M_\odot$	(0.80, 1)	$0.008^{+0.015}_{-0.009}$
	LVC	$1.4868^{+0.0003}_{-0.0003}\,M_\odot$	$1.44^{+0.02}_{-0.02}\,M_\odot$	$3.31^{+0.06}_{-0.05}\,M_\odot$	(0.78, 1)	$0.013^{+0.014}_{-0.013}$

Note. We select parameters most relevant to this study, including the detector-frame binary chirp mass ($\mathcal{M}^{\rm det}$), the source-frame chirp mass ($\mathcal{M}$), the source-frame binary total mass ($m_{\rm tot}$), the mass ratio (q), and the effective spin parameter ($\chi_{\rm eff}$). All quoted numbers are median posterior estimates and 5% lower and 95% upper limits, except q for which the 10%–100% credible interval is given. Source-frame masses are obtained assuming the standard flat ΛCDM cosmology with a Hubble constant $H_0 = 67.9\,\rm km\,s^{-1}\,Mpc^{-1}$ and matter density parameter $\Omega_m = 0.306$ (Ade et al. 2016), except the LVC results for GW170817 where electromagnetic measurements of source redshift are used (Abbott et al. 2019b). All results are based on the `IMRPhenomPv2_NRTidal` waveform model. Additional details for such a comparison are shown in Figures 10–12. Full posterior samples are publicly available at https://github.com/ZhuXJ1/BNSastro.

for $\chi_r > 0.05$. The low probability arises from the fact that the first-born NS is unlikely to get fully recycled, e.g., to achieve spin periods $\lesssim 10$ ms, based on current understanding of BNS formation through isolated binary evolution. We note that the cut on LVC low-spin prior at $\chi = 0.05$ is set as a conservative limit in terms of the NS equation of state. The current spin period of PSR J1946+2052 is 17 ms, for which a dimensionless spin of 0.05 would correspond to an NS radius of $\sim$15 km. (Note that the pulsar is spinning down slowly, likely to 18 ms when the BNS merges in $\sim$46 Myr.) On the other hand, our prior on χ_r is, roughly speaking, marginalized over unknown NS radii over the plausible range of [10, 14] km (Landry et al. 2020).

In Table 2, we summarize posterior estimates of several common source parameters between this work and the LVC results. Our measurements of detector-frame chirp mass $\mathcal{M}^{\rm det}$, source-frame chirp mass $\mathcal{M}$, and total mass $m_{\rm tot}$ are in excellent agreement with LVC results for both events. The only

exception is $\mathcal{M}$ of GW170817, due to different conversions from $\mathcal{M}^{\rm det}$. By incorporating electromagnetic information on the source luminosity distance of GW170817, the measurement uncertainty of $\mathcal{M}$ is reduced by a factor of 2 in Abbott et al. (2019b) from earlier analysis reported in Abbott et al. (2017). Our result agrees well with the latter in this case.

We present the posterior distributions along with priors for the mass ratio q and effective spin parameter $\chi_{\rm eff}$ in Figures 10 and 11, respectively. We find our measurements of q improve upon those of LVC, mildly for GW190425 but considerably for GW170817. This can be understood as follows. Our spin prior is more constraining, as can be seen in Figure 11. Because there is no support for measurable spins in GW170817 as found in Section 3, our prior constraint on $\chi_{\rm eff}$ helps break the $\chi_{\rm eff}$–q degeneracy (see, e.g., Figure 7 in Abbott et al. 2019b). However, we find considerable support of spins for GW190425, but the data are not sufficiently informative to distinguish our prior from that of LVC due to the relatively low
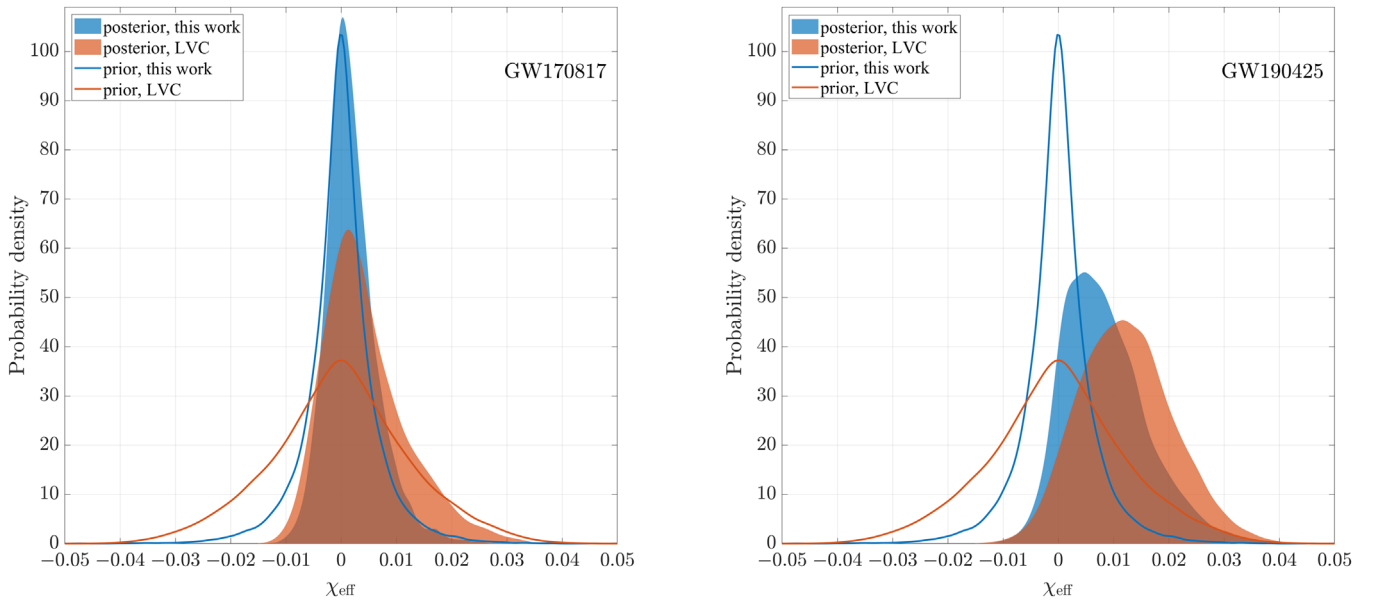
Figure 11. Same as Figure 10, but for the effective spin parameter ($\chi_{\rm eff}$).
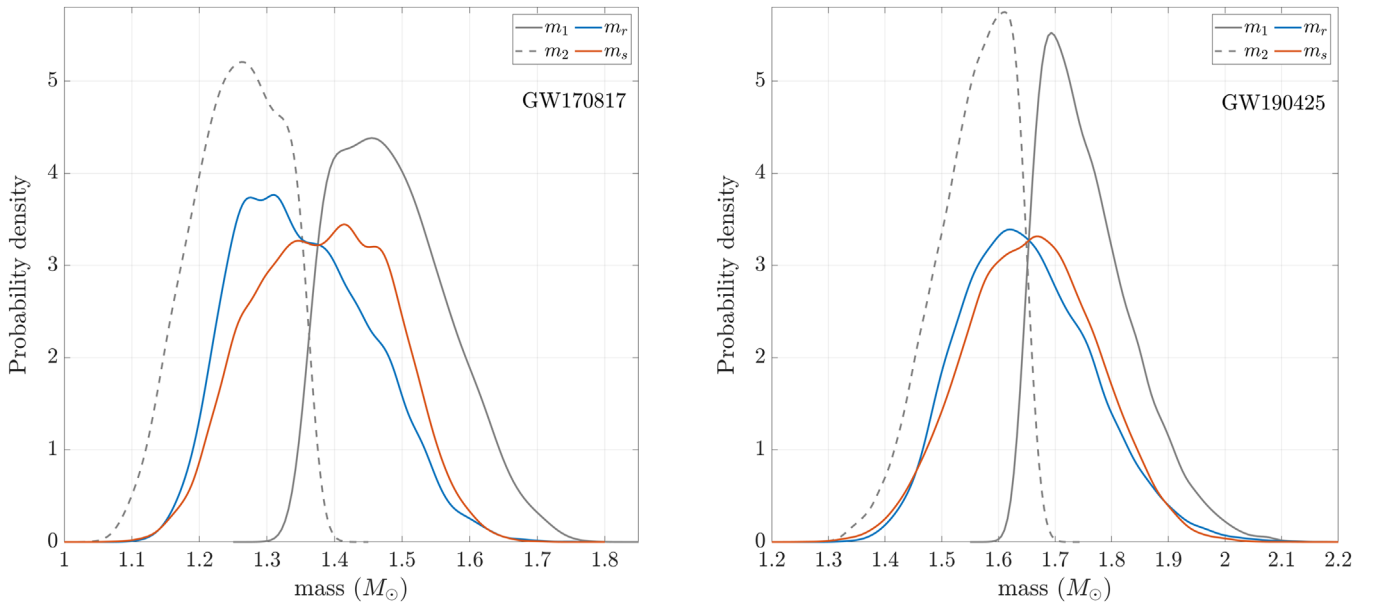
Figure 12. Posterior probability distributions of source-frame component masses for GW170817 (left) and GW190425 (right): (m_r, m_s) derived in this work, and (m_1, m_2) published by the LVC. For GW170817, the LVC only released detector-frame component masses, which are converted to the source frame in the left plot using the redshift $z = 0.009$ of its host galaxy NGC 4993 (Abbott et al. 2017b).

signal-to-noise ratio (12.9). This leads to similar $\chi_{\rm eff}$ posteriors and hence no significant difference in constraints on q. Figure 12 shows the component mass measurements for GW170817 (left) and GW190425 (right).

ORCID iDs

Xing-Jiang Zhu (朱兴江) ⓘ https://orcid.org/0000-0001-7049-6468
Gregory Ashton (艾格瑞) ⓘ https://orcid.org/0000-0001-7288-2231

References

Aasi, J., Abbott, B. P., Abbott, R., et al. 2015, CQGra, 32, 074001
Abbott, B., Abbott, R., Abbott, T., et al. 2017, PhRvL, 119, 161101
Abbott, B. P., Abbott, R., Abbott, T. D., et al. 2017a, ApJL, 850, L39
Abbott, B. P., Abbott, R., Abbott, T. D., et al. 2017b, ApJL, 848, L12
Abbott, B. P., Abbott, R., Abbott, T. D., et al. 2018, LRR, 21, 3
Abbott, B. P., Abbott, R., Abbott, T. D., et al. 2019a, PhRvX, 9, 031040
Abbott, B. P., Abbott, R., Abbott, T. D., et al. 2019b, PhRvX, 9, 011001
Abbott, B. P., Abbott, R., Abbott, T. D., et al. 2020a, ApJL, 892, L3
Abbott, R., Abbott, T. D., Abraham, S., et al. 2020b, PhRvD, 102, 043015
Abbott, R., Abbott, T. D., Abraham, S., et al. 2020c, ApJL, 896, L44
Acernese, F., Agathos, M., Agatsuma, K., et al. 2015, CQGra, 32, 024001
Ade, P. A. R., Aghanim, N., Arnaud, M., et al. 2016, A&A, 594, A13
Alpar, M. A., Cheng, A. F., Ruderman, M. A., & Shaham, J. 1982, Natur, 300, 728
Alsing, J., Silva, H. O., & Berti, E. 2018, MNRAS, 478, 1377
Anderson, S. B., Gorham, P. W., Kulkarni, S. R., Prince, T. A., & Wolszczan, A. 1990, Natur, 346, 42
Andrews, J. J. 2020, ApJL, 900, L41
Andrews, J. J., & Mandel, I. 2019, ApJL, 880, L8
Antoniadis, J., Tauris, T. M., Ozel, F., et al. 2016, arXiv:1605.01665
Arzoumanian, Z., Cordes, J. M., & Wasserman, I. 1999, ApJ, 520, 696

Ashton, G., Hübner, M., Lasky, P. D., et al. 2019, ApJS, 241, 27
Bae, Y.-B., Kim, C., & Lee, H. M. 2014, MNRAS, 440, 2714
Bailes, M. 1988, A&A, 202, 109
Bailes, M., Jameson, A., Abbate, F., et al. 2020, PASA, 37, e028
Belczynski, K., Askar, A., Arca-Sedda, M., et al. 2018, A&A, 615, A91
Bhattacharya, D., & van den Heuvel, E. P. J. 1991, PhR, 203, 1
Biwer, C. M., Capano, C. D., De, S., et al. 2019, PASP, 131, 024503
Blanchard, P. K., Berger, E., Fong, W., et al. 2017, ApJL, 848, L22
Bransgrove, A., Levin, Y., & Beloborodov, A. 2018, MNRAS, 473, 2771
Burgay, M., D'Amico, N., Possenti, A., et al. 2003, Natur, 426, 531
Cameron, A. D., Champion, D. J., Kramer, M., et al. 2018, MNRAS, 475, L57
Cameron, A. D., Li, D., Hobbs, G., et al. 2020, MNRAS, 495, 3515
Chattopadhyay, D., Stevenson, S., Hurley, J. R., Rossi, L. J., & Flynn, C. 2020,
    MNRAS, 494, 1587
Contopoulos, I., Kazanas, D., & Fendt, C. 1999, ApJ, 511, 351
Corongiu, A., Kramer, M., Stappers, B. W., et al. 2007, A&A, 462, 703
Cromartie, H. T., Fonseca, E., Ransom, S. M., et al. 2020, NatAs, 4, 72
De Loore, C., de Greve, J. P., & de Cuyper, J. P. 1975, Ap&SS, 36, 219
Delgado, A. J., & Thomas, H. C. 1981, A&A, 96, 142
Dewi, J. D. M., & Pols, O. R. 2003, MNRAS, 344, 629
Dietrich, T., Bernuzzi, S., & Tichy, W. 2017a, PhRvD, 96, 121501
Dietrich, T., Khan, S., Dudi, R., et al. 2019, PhRvD, 99, 024029
Dietrich, T., Ujevic, M., Tichy, W., Bernuzzi, S., & Brügmann, B. 2017b,
    PhRvD, 95, 024029
Farrow, N., Zhu, X.-J., & Thrane, E. 2019, ApJ, 876, 18
Ferdman, R. D., Freire, P. C. C., Perera, B. B. P., et al. 2020, Natur, 583, 211
Ferdman, R. D., Stairs, I. H., Kramer, M., et al. 2013, ApJ, 767, 85
Ferdman, R. D., Stairs, I. H., Kramer, M., et al. 2014, MNRAS, 443, 2183
Flannery, B. P., & van den Heuvel, E. P. J. 1975, A&A, 39, 61
Fonseca, E., Stairs, I. H., & Thorsett, S. E. 2014, ApJ, 787, 82
Gao, H., Cao, Z., Ai, S., & Zhang, B. 2017, ApJL, 851, L45
Ghosh, P., & Lamb, F. K. 1979, ApJ, 234, 296
Goldreich, P., & Julian, W. H. 1969, ApJ, 157, 869
Goldreich, P., & Reisenegger, A. 1992, ApJ, 395, 250
Grindlay, J., Portegies Zwart, S., & McMillan, S. 2006, NatPh, 2, 116
Haniewicz, H. T., Ferdman, R. D., Freire, P. C. C., et al. 2020, arXiv:2007.
    07565
Hannam, M., Schmidt, P., Bohé, A., et al. 2014, PhRvL, 113, 151101
Hills, J. G. 1983, ApJ, 267, 322
Ivanova, N., Belczynski, K., Kalogera, V., Rasio, F. A., & Taam, R. E. 2003,
    ApJ, 592, 475
Jacoby, B. A., Cameron, P. B., Jenet, F. A., et al. 2006, ApJL, 644, L113
Janssen, G. H., Stappers, B. W., Kramer, M., et al. 2008, A&A, 490, 753
Kalogera, V., Belczynski, K., Kim, C., O'Shaughnessy, R., & Willems, B.
    2007, PhR, 442, 75
Keith, M. J., Kramer, M., Lyne, A. G., et al. 2009, MNRAS, 393, 623
Khan, S., Husa, S., Hannam, M., et al. 2016, PhRvD, 93, 044007
Kiziltan, B., Kottas, A., de Yoreo, M., & Thorsett, S. E. 2013, ApJ, 778, 66
Kramer, M. 1998, ApJ, 509, 856
Kramer, M., Stairs, I. H., Manchester, R. N., et al. 2006, Sci, 314, 97
Kruckow, M. U. 2020, A&A, 639, A123
Lai, D., Chernoff, D. F., & Cordes, J. M. 2001, ApJ, 549, 1111
Landry, P., Essick, R., & Chatziioannou, K. 2020, PhRvD, 101, 123007
Lattimer, J. M., & Prakash, M. 2001, ApJ, 550, 426
Lattimer, J. M., & Schutz, B. F. 2005, ApJ, 629, 979
Lazarus, P., Brazier, A., Hessels, J. W. T., et al. 2015, ApJ, 812, 81
Lee, W. H., Ramirez-Ruiz, E., & van de Ven, G. 2010, ApJ, 720, 953
Lorimer, D. R., Bailes, M., Dewey, R. J., & Harrison, P. A. 1993, MNRAS,
    263, 403
Lorimer, D. R., & Kramer, M. 2005, Handbook of Pulsar Astronomy, Vol. 4
    (Cambridge: Cambridge Univ. Press)
Lynch, R. S., Freire, P. C. C., Ransom, S. M., & Jacoby, B. A. 2012, ApJ,
    745, 109
Lynch, R. S., Swiggum, J. K., Kondratiev, V. I., et al. 2018, ApJ, 859, 93
Lyne, A. G., Burgay, M., Kramer, M., et al. 2004, Sci, 303, 1153
Manchester, R. N., Hobbs, G. B., Teoh, A., & Hobbs, M. 2005, AJ, 129, 1993
Mandel, I., Mueller, B., Riley, J., et al. 2020, arXiv:2007.03890
Mapelli, M., & Giacobbo, N. 2018, MNRAS, 479, 4391
Marshall, F. E., Gotthelf, E. V., Middleditch, J., Wang, Q. D., & Zhang, W.
    2004, ApJ, 603, 682
Martinez, J. G., Stovall, K., Freire, P. C. C., et al. 2015, ApJ, 812, 143
Martinez, J. G., Stovall, K., Freire, P. C. C., et al. 2017, ApJL, 851, L29
Massevitch, A. G., Tutukov, A. V., & Iungelson, L. R. 1976, Ap&SS, 40, 115
Metzger, B. D., Thompson, T. A., & Quataert, E. 2018, ApJ, 856, 101
Neijssel, C. J., Vigna-Gómez, A., Stevenson, S., et al. 2019, MNRAS,
    490, 3740
Ng, C., Kruckow, M. U., Tauris, T. M., et al. 2018, MNRAS, 476, 4315
Ostriker, J. P., & Gunn, J. E. 1969, ApJ, 157, 1395
Özel, F., Psaltis, D., Narayan, R., & Santos Villarreal, A. 2012, ApJ, 757, 55
Pankow, C. 2018, ApJ, 866, 60
Pejcha, O., Thompson, T. A., & Kochanek, C. S. 2012, MNRAS, 424, 1570
Peters, P. C. 1964, PhRv, 136, 1224
Phinney, E. S. 1991, ApJL, 380, L17
Phinney, E. S., & Sigurdsson, S. 1991, Natur, 349, 220
Popov, S. B., & Turolla, R. 2012, Ap&SS, 341, 457
Postnov, K. A., & Yungelson, L. R. 2014, LRR, 17, 3
Prince, T. A., Anderson, S. B., Kulkarni, S. R., & Wolszczan, A. 1991, ApJL,
    374, L41
Radhakrishnan, V., & Srinivasan, G. 1982, CSci, 51, 1096
Romani, R. W. 1990, Natur, 347, 741
Romero-Shaw, I. M., Farrow, N., Stevenson, S., Thrane, E., & Zhu, X.-J. 2020,
    MNRAS, 496, L64
Safarzadeh, M., Ramirez-Ruiz, E., & Berger, E. 2020, ApJ, 900, 13
Schwab, J., Podsiadlowski, P., & Rappaport, S. 2010, ApJ, 719, 722
Siegel, D. M., & Metzger, B. D. 2018, ApJ, 858, 52
Smarr, L. L., & Blandford, R. 1976, ApJ, 207, 574
Smith, R., Ashton, G., Vajpeyi, A., & Talbot, C. 2019, arXiv:1909.11873
Speagle, J. S. 2020, MNRAS, 493, 3132
Spitkovsky, A. 2006, ApJL, 648, L51
Srinivasan, G., & van den Heuvel, E. P. J. 1982, A&A, 108, 143
Stovall, K., Freire, P. C. C., Chatterjee, S., et al. 2018, ApJL, 854, L22
Swiggum, J. K., Rosen, R., McLaughlin, M. A., et al. 2015, ApJ, 805, 156
Taam, R. E., & van den Heuvel, E. P. J. 1986, ApJ, 305, 235
Tauris, T. M., Kramer, M., Freire, P. C. C., et al. 2017, ApJ, 846, 170
Tauris, T. M., Langer, N., & Podsiadlowski, P. 2015, MNRAS, 451, 2123
The LIGO Scientific Collaboration and The Virgo Collaboration 2020, GW
    Open Science Center, GW190425 Data Products (doi:10.7935/ggb8-1v94)
van den Heuvel, E. P. J. 2017, JApA, 38, 45
van Leeuwen, J., Kasian, L., Stairs, I. H., et al. 2015, ApJ, 798, 118
Veitch, J., Raymond, V., Farr, B., et al. 2015, PhRvD, 91, 042003
Vink, J. 2008, AdSpR, 41, 503
Weisberg, J. M., Nice, D. J., & Taylor, J. H. 2010, ApJ, 722, 1030
Wysocki, D., O'Shaughnessy, R., Wade, L., & Lange, J. 2020, arXiv:2001.
    01747
Ye, C. S., Fong, W.-f., Kremer, K., et al. 2020, ApJL, 888, L10
Zhang, L., Li, D., Hobbs, G., et al. 2019, ApJ, 877, 55
Zhu, X., Thrane, E., Osłowski, S., Levin, Y., & Lasky, P. D. 2018, PhRvD, 98,
    043002